Water Research 203 (2021) 117561

Contents lists available at ScienceDirect

Water Research

journal homepage: www.elsevier.com/locate/watres

Colloidal stability of nanosized activated carbon in aquatic systems: Effects of pH, electrolytes, and macromolecules

Zhiwei Shao [a], Shijie Luo [a], Miaoting Liang [a], Zengping Ning [b], Weimin Sun [c,d], Yujing Zhu [a], Juncheng Mo [a], Yongtao Li [a], Weilin Huang [e], Chengyu Chen [a,*]

[a] College of Natural Resources and Environment, South China Agricultural University, 483 Wushan Road, Guangzhou, Guangdong 510642, China
[b] State Key Laboratory of Environmental Geochemistry, Chinese Academy of Sciences, 99 Linchengxi Road, Guiyang 550081, China
[c] National-Regional Joint Engineering Research Center for Soil Pollution Control and Remediation in South China, Guangdong Key Laboratory of Integrated Agro-environmental Pollution Control and Management, Institute of Eco-environmental and Soil Sciences, Guangdong Academy of Sciences, Guangzhou 510650, China
[d] School of Environment, Henan Key Laboratory for Environmental Pollution Control, Key Laboratory for Yellow River and Huai River Water Environment and Pollution Control, Ministry of Education, Henan Normal University, Xinxiang, Henan 453007, China
[e] Department of Environmental Sciences, Rutgers, The State University of New Jersey, 14 College Farm Road, New Brunswick, NJ 08901, United States

ARTICLE INFO

Keywords:
Aggregation kinetics
Attachment efficiency
DLVO theory
Steric hindrance
Cation bridging
Surface water environments

ABSTRACT

Nanosized activated carbon (NAC) is a novel adsorbent with great potential for water reclamation. However, its transport and reactivity in aqueous environments may be greatly affected by its stability against aggregation. This study investigated the colloidal stability of NAC in model aqueous systems with broad background solution chemistries including 7 electrolytes (NaCl, $NaNO_3$, Na_2SO_4, KCl, $CaCl_2$, $MgCl_2$, and $BaCl_2$), pH 4–9, and 6 macromolecules (humic acid (HA), fulvic acid (FA), cellulose (CEL), bovine serum albumin (BSA), alginate (ALG), and extracellular polymeric substance (EPS)), along with natural water samples collected from pristine to polluted rivers. The results showed that higher solution pH stabilized NAC by raising the critical coagulation concentration from 28 to 590 mM NaCl. Increased cation concentration destabilized NAC by charge screening, with the cationic influence following $Ba^{2+} > Ca^{2+} > Mg^{2+} >> Na^{+} > K^{+}$. Its aggregation behavior could be predicted with the Derjaguin-Landau-Verwey-Overbeek (DLVO) theory with a Hamaker constant (A_{CWC}) of 4.3×10^{-20} J. The presence of macromolecules stabilized NAC in NaCl solution and most $CaCl_2$ solution following EPS > BSA > CEL > HA > FA > ALG, due largely to enhanced electrical repulsion and steric hindrance originated from adsorbed macromolecules. However, ALG and HA strongly destabilized NAC via cation bridging at high Ca^{2+} concentrations. Approximately half of NAC particles remained stably suspended for ~10 d in neutral freshwater samples. The results demonstrated the complex effects of water chemistry on fate and transport of NAC in aquatic environments.

1. Introduction

Nanosized activated carbon (NAC) is a novel carbonaceous engineered nanomaterial (ENM) possessing unique nano-dimension, extremely porous structure, enormous specific surface area (SSA), varied surface functionality, and highly hydrophobic nature (Chen and Huang, 2017; Chen et al., 2017; Nazem et al., 2020). The sizes of NAC are much smaller than conventional powdered activated carbon (PAC) (10–50 μm mean diameter) and granular activated carbon (GAC), and are similar with or smaller than super-fine PAC (SPAC) (roughly 0.1–1 μm mean diameter) (Bonvin et al., 2016; Partlan et al., 2016). Previous studies have demonstrated the potential applicability of NAC as adsorbents and nanofiltration membranes in water treatment processes (Chen et al., 2017; Hosseini et al., 2018). Besides, NAC is widely considered in other fields as potential candidates for antimicrobial agents (Lakshmi et al., 2018), catalyst support (Abdulkareem-Alsultan et al., 2016), and drug carriers (Sengupta et al., 2014). Direct use of NAC for water treatment or unintentional release of NAC during other application activities could introduce such ENM into natural and engineered aquatic systems. Although limited research shows that NAC exhibited insignificant cytotoxicity after short-term exposure (Sengupta et al., 2014), it may act as strong pollutant carriers during environmental transport (Vidal et al., 2008). Therefore, understanding the fate and transport of NAC in various aqueous environments is crucial for

* Corresponding author.
E-mail address: cychen@scau.edu.cn (C. Chen).

https://doi.org/10.1016/j.watres.2021.117561
Received 18 June 2021; Received in revised form 8 August 2021; Accepted 11 August 2021
Available online 16 August 2021

designing its application schemes for water treatment as well as evaluating its potential ecological and health risks.

Upon release of NAC nanomaterials into aquatic environments, both their transport and reactivity are largely dependent on the aggregation behavior, which would alter their size and SSA, adsorption capacity, environmental toxicity, and ultimate fate (Hewitt et al., 2020). The existing literature on fate and transport of carbonaceous ENM focuses mainly on fullerene (C_{60}) (Kyzyma et al., 2019), carbon nanotubes (CNTs) (single-walled, SWCNTs and multi-walled, MWCNTs) (Xia et al., 2019), and graphene oxide (GO) (Ali et al., 2020), yet much less attention was paid to the novel NAC nanomaterial. Our previous studies have demonstrated the potent advantages including excellent adsorption capacity (Chen et al., 2017) and colloidal stability (Chen and Huang, 2017) simultaneously possessed by NAC, making it suitable for emergent contamination treatment and in situ groundwater remediation. It was shown that considering solely the effects of NaCl or $CaCl_2$, four different model NACs (two made from bamboo and trees, and others made from coconut shell and bamboo charcoals) exhibited strong colloidal stability under freshwater conditions at low salt concentrations; while they aggregated under seawater conditions at higher salt concentrations with behaviors predictable by the Derjaguin-Landau-Verwey-Overbeek (DLVO) theory, from which their Hamaker constants were derived (Chen and Huang, 2017).

However, natural aquatic environments contain complex solution chemistries including various electrolytes, pH, and macromolecules (Saleh et al., 2010). It remains unclear how these environmental factors exert single and combined effects on the aggregation kinetics of NAC. Environmental and biological macromolecules, such as natural organic matter (NOM), polysaccharides, proteins, and extracellular polymeric substance (EPS), having different molecular size, structure, and functionality are ubiquitously distributed in aqueous environments (Liu et al., 2020). As our previous study showed that NAC with large SSA and hydrophobic surface had strong adsorption affinity to organic pollutants (Chen et al., 2017), we hypothesized that macromolecules would also interact with NAC and adsorb onto particle surface. Depending on the solution composition and concentration of electrolytes and macromolecules, these environmental factors may promote or inhibit the aggregation process of NAC, as have been shown to vary among different carbonaceous ENMs (e.g., CNTs Liu et al. 2016 and fullerene Zhang et al. 2013). Moreover, these ENMs may also exhibit different aggregation behaviors in model and real water samples (Chowdhury et al., 2013). To date, previous research only reported the single influence of NaCl or $CaCl_2$ on aggregation kinetics of NAC without macromolecules and only in model aqueous systems (Chen and Huang, 2017). Therefore, complex model solutions and natural water samples should be included to elucidate the aggregation behavior of NAC and its interaction mechanism with macromolecules in aqueous environments.

The objective of this study was to investigate the single and combined effects of solution chemistry including electrolytes, pH, and macromolecules on the colloidal stability of NAC in model and natural aqueous solutions. The following environmental scenarios were considered: (1) various electrolytes and pH levels; (2) different macromolecules in NaCl and $CaCl_2$ solutions; (3) interaction mechanism of NAC with macromolecules; (4) natural water samples with various solution chemistry; and (5) early-stage vs. long-term stability of NAC. The model solutions contained 7 electrolytes (NaCl, $NaNO_3$, Na_2SO_4, KCl, $CaCl_2$, $MgCl_2$, or $BaCl_2$) at concentrations (0.01–1000 mM) typically found in aqueous environments, pH 4–9, and 6 macromolecules. A hydrophobic and semi-rigid humic acid (HA) and a fulvic acid (FA) with smaller molecular weight and shorter carbon chain were selected as two model NOM (Ali et al., 2020); two polysaccharides included a hydrophilic cellulose (CEL) with linear chain of D-glucose units (Updegraff, 1969) and a hydrophilic, linear, and semi-flexible alginate (ALG) (Chen et al., 2019); bovine serum albumin (BSA) was used as a hydrophobic and globular protein (Saleh et al., 2010); and an EPS composed of polysaccharide and protein having random coils with partially extended chains was extracted for study (Liu et al., 2020). Freshwater samples from natural rivers possessing different solution chemistries ranging from acidic/contaminated to neutral/clean conditions were also collected for comparison of NAC stability in model and natural water. The results demonstrated the complex role of electrolytes, pH, and macromolecules on the fate and transport of NAC in aquatic environments.

2. Materials and methods

2.1. NAC stock suspension

Super activated carbon nanoparticles (stock # US1077) were obtained from US Research Nanomaterials, Inc. (Houston, USA). Our previous studies have characterized its aggregation (Chen and Huang, 2017) and adsorption (Chen et al., 2017) behaviors with the designation of NAC4. Its stock suspension was previously prepared via natural sedimentation (Chen and Huang, 2017), which was replaced here by centrifugation as described in S1.1 of the Supplementary Material. This method yielded small intensity-weighed hydrodynamic diameter (D_h), uniform size distribution (i.e., polydispersity index (PDI)) (Fig. S1a), and high particle concentration (Fig. S1b). The NAC concentration of stock suspension (358.0 ± 9.8 mg/L (Table S1)) was measured gravimetrically.

2.2. Preparation of model and natural aqueous solutions

Monovalent (NaCl, $NaNO_3$, Na_2SO_4, and KCl) and divalent ($CaCl_2$, $MgCl_2$, and $BaCl_2$) salts (ACS grade) were purchased from Titan Scientific Co., Ltd (Shanghai, China). Suwannee River HA (Standard II) and FA (Standard I) were purchased from International Humic Substances Society (St. Paul, MN); CEL, BSA, and ALG with Cat. No. of C5013, A7030, and 1,80,947, respectively, were obtained from Sigma Aldrich (Shanghai, China); EPS was extracted from culture medium of *Shewanella oneidensis* MR-1. The total organic carbon (TOC) concentrations (mg_C/L, i.e., milligram TOC per liter) of macromolecule stock solutions are presented in Table 1.

Six natural water (NW) samples were collected from Dajiagou River and Chahe River (Guizhou, China), with the sampling map and geographic coordinates shown in Fig. S2 and Table 2. Detailed methods for extracting EPS and preparing the above model and natural aqueous solutions are described in S1.2 of the Supplementary Material.

2.3. Characterization of NAC

The D_h of NAC in different solutions was determined with dynamic light scattering (DLS) using a Zetasizer Nano ZS90 instrument (Malvern Instruments Ltd, UK). Triplicate samples were each measured 10 times for electrophoretic mobility that was converted to zeta (ζ) potential using Eq. (S1). The NAC before and after contact with macromolecules and $CaCl_2$ were examined for its aggregation state and morphology

Table 1
Total organic carbon (TOC) concentration in each macromolecule stock solution, and the adsorbed macromolecule amount (q_e) onto NAC. The adsorption experiments were conducted at 600 mg/L macromolecules, 30 mg/L NAC, 1 mM NaCl, 25 °C, and pH 6. The unit of mg_C refers to milligram TOC.

Macromolecule	TOC concentration in 600 mg/L stock solution		Adsorption amount by NAC
	TOC (mg_C/L)	TOC (%$_w$)	q_e (mg_C/g)
HA	277.8 ± 20.4	46.3 ± 3.4	29.0 ± 1.8
FA	265.8 ± 0.1	44.3 ± 0.02	50.8 ± 5.2
CEL	168.0 ± 7.8	28.0 ± 1.3	18.8 ± 3.6
BSA	215.4 ± 3.6	35.9 ± 0.6	76.1 ± 2.3
ALG	151.8 ± 0.1	25.3 ± 0.01	47.7 ± 5.8
EPS	174.0 ± 3.6	29.0 ± 0.6	46.8 ± 4.9

Table 2
Information of the natural water (NW) samples collected at sampling sites 1 to 6.

Sample	NW1	NW2	NW3	NW4	NW5	NW6
North latitude	25°48′34.73′′	25°48′29.52′′	25°48′18.76′′	25°48′06.40′′	25°48′05.69′′	25°47′56.49′′
East longitude	107°37′09.16′′	107°37′02.32′′	107°37′02.23′′	107°37′57.60′′	107°37′56.05′′	107°37′08.37′′
TOC (mg_C/L)[a]	0.5460	1.175	41.92	16.28	1.197	3.417
pH	2.60	2.68	5.21	8.25	8.69	8.80
Experimental pH[b]	2.62	2.70	5.23	7.60	7.66	7.67
E_h (mV)[c]	358.8	359.6	251.1	107.8	65.60	54.70
Conductivity (μS/cm)	1406	1413	1400	528.0	244.0	307.0
T (°C)	22.50	22.50	23.50	24.20	25.40	25.70
IS (mM)[d]	65.21	61.10	50.89	15.61	5.693	7.541
Na^+ (mM)	0.06304	0.04913	0.2109	0.09090	0.1374	0.1282
K^+ (mM)	0.08487	0.09103	0.08180	0.05051	0.08282	0.07513
Ca^{2+} (mM)	4.397	4.449	13.04	3.790	1.236	1.726
Mg^{2+} (mM)	4.929	4.998	0.02000	0.2000	0.6000	0.5150
Mn^{2+} (mM)	0.06040	0.05720	–	–	–	–
Al^{3+} (mM)	1.861	1.864	0.03235	0.01588	0.0005880	0.005882
Fe^{3+} (mM)	0.9488	0.9618	0.003750	0.0001790	0.0001790	0.0005357
F^- (mM)	0.2216	0.1679	0.2321	0.02316	–	0.008947
Cl^- (mM)	0.03437	0.02451	0.1552	0.07437	0.1039	0.09775
NO_3^- (mM)	0.02565	–	0.01226	0.02726	0.02258	0.04694
SO_4^{2-} (mM)	16.79	14.61	12.13	3.713	0.9221	1.429

[a] The unit of mg_C/L refers to milligram TOC per liter;.
[b] Experimental pH of NW samples after diluted by 5% using NAC suspension;.
[c] E_h = oxidation–reduction potential;.
[d] IS = ionic strength calculated for all ions according to $IS = \frac{1}{2}\sum c_i z_i^2$, where c_i and z_i are the ionic concentration and charge, respectively, of ion i. The ionic concentrations were diluted by 5% after mixing with NAC suspension.

under transmission electron microscope (TEM). The long-term stability of NAC in model and natural solutions was measured by light absorbance and visual observation. Detailed characterization methods are described in S1.3 of the Supplementary Material.

2.4. Determination of aggregation kinetics

The experimental conditions for measuring the aggregation behaviors of NAC in electrolyte solutions, macromolecule solutions, and NW samples, along with their reasons of choice, are described in Tables S2, S3, and S1.4 of the Supplementary Material. The aggregation kinetics of NAC were measured with the Zetasizer instrument using time-resolved DLS technique (Li et al., 2021) as described in S1.5 of the Supplementary Material. The early-stage aggregation rate (k) was determined with Eq. S2. The attachment efficiency (α) ranging from 0 (no aggregation) to 1 (fast aggregation) was employed to quantify the colloidal stability (Eq. S3). The critical coagulation concentration (CCC), which represents the minimum electrolyte concentration to induce diffusion-limited particle aggregation, was determined on the stability profile from the intersection of extrapolated lines through the diffusion- and reaction-limited regimes (Chowdhury et al., 2013). The experimental α data determined in NaCl solution at pH 6 were fitted by the theoretical α values calculated based on the DLVO theory (Eqs. (S4)–(S12)) (S1.6 of the Supplementary Material).

2.5. Macromolecule adsorption by NAC

The adsorption of macromolecules onto NAC was determined by one-point batch adsorption experiment following a method modified from previous studies (Chen et al., 2019; Zhang et al., 2013), as described in S1.7 of the Supplementary Material. The adsorption experiment was conducted at 600 mg/L macromolecules, 30 mg/L NAC, 1 mM NaCl, 25 °C, and pH 6. Higher macromolecule and NAC concentrations were used in adsorption experiments to ensure the measurement accuracy and precision.

3. Results and discussion

3.1. Effects of pH and electrolyte

The D_h of NAC measured at 1 mM NaCl continuously decreased as pH increased from 2 to 4, which corresponded to the enhanced negative charge of NAC, yielding a point of zero charge near pH 2 (Fig. S3). The colloidal stability of NAC as a function of pH was quantified in NaCl solutions (Fig. 1a). All stability curves display two aggregation regimes predictable by the DLVO theory (Chen and Huang, 2017): reaction-limited aggregation regime ($\alpha < 1$) at electrolyte concentrations below CCC, and the diffusion-limited regime ($\alpha = 1$) at electrolyte concentrations above CCC. The stability curves continuously shifted rightwards at higher pH in NaCl solution, indicating enhanced colloidal stability of NAC. The CCC values increased by ~21 times from 28 to 590 mM NaCl as pH changed from 4 to 9. This phenomenon occurred due to the deprotonation of acidic functional groups on NAC at higher pH that inhibited aggregation (László et al., 2004, 2007). The results demonstrated the strong impact of pH on stability of NAC especially under acidic conditions.

The ζ potential of NAC as a function of electrolyte concentration was determined at pH 6 for different monovalent and divalent electrolytes (Fig. 1b). The two groups of electrolytes clearly showed separate regimes of ζ potentials, with each group displaying overlapped trends that all increased with electrolyte concentration. The cationic valence exhibited strong charge screening effect on NAC, rather than the type of ions given the same valence. The change in ζ potential with electrolyte concentration was attributed to compressed electrical double layer (Yang et al. 2017). Divalent electrolytes exerted stronger screening effect due to their higher charge density in the diffuse layer and possibly their specific adsorption on NAC surface as compared with monovalent electrolytes (Saleh et al., 2008). For instance, the ζ potentials were −43.9 and −3.1 mV at 10 mM $NaNO_3$ and $BaCl_2$, respectively. Specifically, Na_2SO_4 exhibited a trend slightly above other 1:1 electrolyte since it contains two Na^+. The ionic strength (IS) was one of the determining parameters as seen in the Debye-Hückel parameter (Eq. S11). Under seawater concentrations, the negative charge was almost completely screened by all cations.

The stability curves of NAC in different electrolyte solutions at pH 6

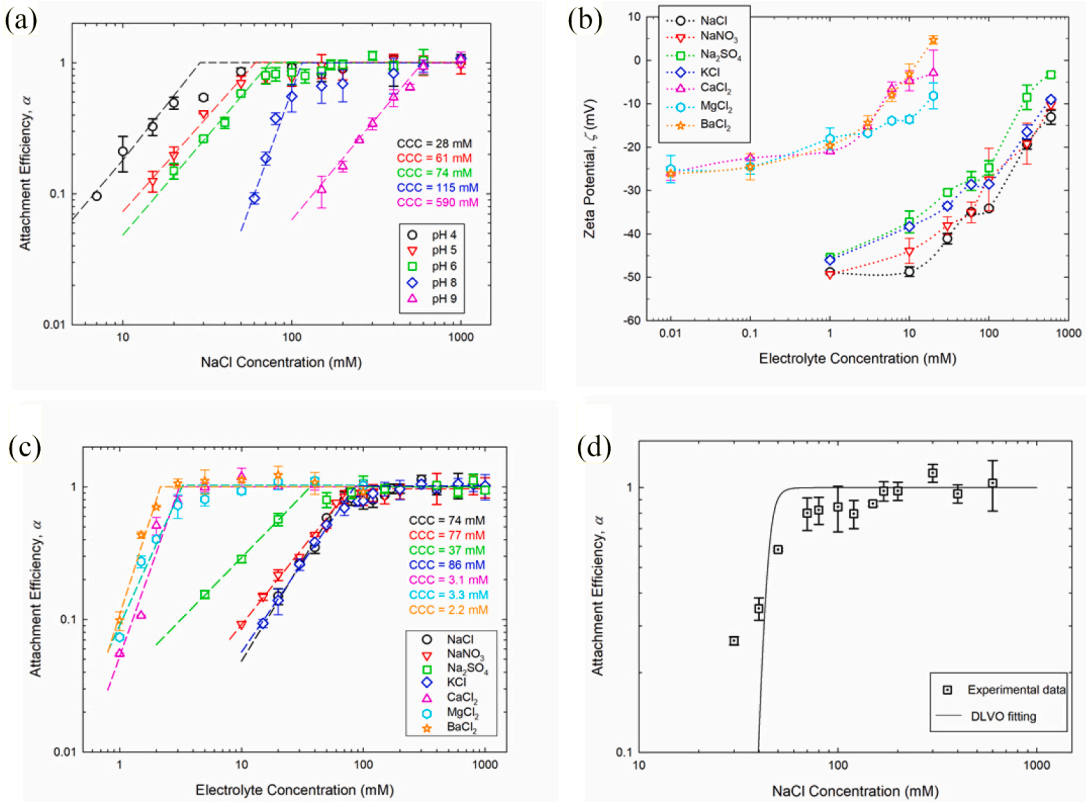

Fig. 1. Influence of pH and electrolytes on stability of NAC: (a) Attachment efficiency as a function of NaCl concentration at different pH; (b) zeta potential and (c) attachment efficiency as a function of monovalent and divalent electrolyte concentrations at pH 6. The dashed lines are extrapolated from the reaction- and diffusion-limited aggregation regimes, and their intersections yielded the critical coagulation concentration (CCC) values. The dotted lines are only for visual guidance. (d) DLVO theoretical fitting (solid line) for experimental attachment efficiency (data point) of NAC in NaCl solution at pH 6 according to Eq. S4. The fitting yielded a Hamaker constant for NAC in water (A_{CWC}) of 4.3×10^{-20} J. All experiments were conducted at 10 mg/L NAC and 25 °C. The error bars represent standard deviations from triplicate samples.

all exhibited two distinct aggregation regimes (Fig. 1c). The CCC values for divalent electrolytes were much lower than those for monovalent electrolytes, indicating that divalent electrolytes were more effective in inducing NAC aggregation, which corresponded to the ζ potential results in Fig. 1b. This result is consistent with other ENMs including C_{60} (Chen and Elimelech, 2007), SWCNTs (Saleh et al., 2010), and MWCNTs (Yang et al., 2017).

The CCC values were close among NaCl (74 mM), $NaNO_3$ (77 mM), and KCl (86 mM), which were approximately twice as that for Na_2SO_4 (37 mM, equivalent to 74 mM Na^+ counter ions). The CCC values for 3 divalent electrolytes were ~3 mM, providing a ratio of CCC values in $CaCl_2$ and NaCl proportional to $\sim 2^{-4.6}$, which followed the Schulze-Hardy rule ranging from 2^{-2} to 2^{-6} (Tang et al., 2017). The results again suggest that the influence of electrolytes on stability of NAC mainly arises from cationic valence. Overall, the potential for inducing NAC aggregation by cations followed the order of $Ba^{2+} > Ca^{2+} > Mg^{2+} >> Na^+ > K^+$, noting that charge screening and even reversal occurred at high Ca^{2+} and Ba^{2+} concentrations (Fig. 1b). This was likely attributed to the specific binding of Ca^{2+} and Ba^{2+} to NAC that led to significant destabilization, as previously observed for black carbon (Xu et al., 2017). Furthermore, this order of inducing NAC aggregation was inversely correlated to the hydration force of divalent cations ($Mg^{2+} > Ca^{2+} > Ba^{2+}$), which would reduce their interaction with nanoparticles (Wang et al., 2017).

Fig. 1d shows that the theoretical simulation based on the DLVO theory (Eqs. S4–S12) generally fitted through the experimental stability data in NaCl solution. This fitting process derived the Hamaker constants of NAC in water (A_{CWC}) and vacuum (A_{CC}) of 4.3×10^{-20} and 16×10^{-20} J, respectively. These values are greater than those previously reported for NAC prepared via natural sedimentation (Chen and Huang, 2017) as compared in Table S4. The aggregation behavior of NAC only induced slight influence on its SSA, which gradually decreased from 610 m^2/g in Milli-Q water to 604 and 601 m^2/g in 2 and 25 mM $CaCl_2$ solutions, respectively (Table S5). In summary, Fig. S4 illustrates the combined effects of solution pH and electrolyte concentration, showing that the aggregation rate of NAC enhanced with increasing electrolyte concentration and decreasing pH.

3.2. *Stability in electrolyte solution at fixed macromolecule concentration*

3.2.1. *NaCl solutions*

The ζ potentials of NAC in the absence or presence of 10 mg_C/L (milligram TOC per liter) macromolecules were determined at varying concentrations of NaCl (Fig. 2a). Despite the presence of macromolecules, the ζ potentials all became less negative as electrolyte concentrations increased. Among 6 macromolecules, BSA was the most effective in reducing the negative ζ potential of NAC in NaCl solution (Fig. 2a). Meanwhile, BSA also exhibited the strongest adsorption ($q_e = 76.1 \pm 2.3$ mg_C/g (milligram TOC per gram) (Table 1)) onto NAC, which had hydrophobic surface and large SSA (Table S5). With an isoelectric point of 4.7, BSA was negatively charged at pH 6 (Kopac et al., 2018) and so was the NAC surface (Fig. 2a). To prevent the buildup of electrostatic potential, co-adsorption of solution cations (e.g., Na^+ and Ca^{2+}) into the interfacial film between the shear plane and particle surface occurred, resulting in reduction of ζ potential. The strong adsorption of BSA and development of protein corona on nanoparticles was also observed for MWCNTs (Kopac et al., 2018), soot (Chen et al., 2019), and plastic (Liu et al., 2020).

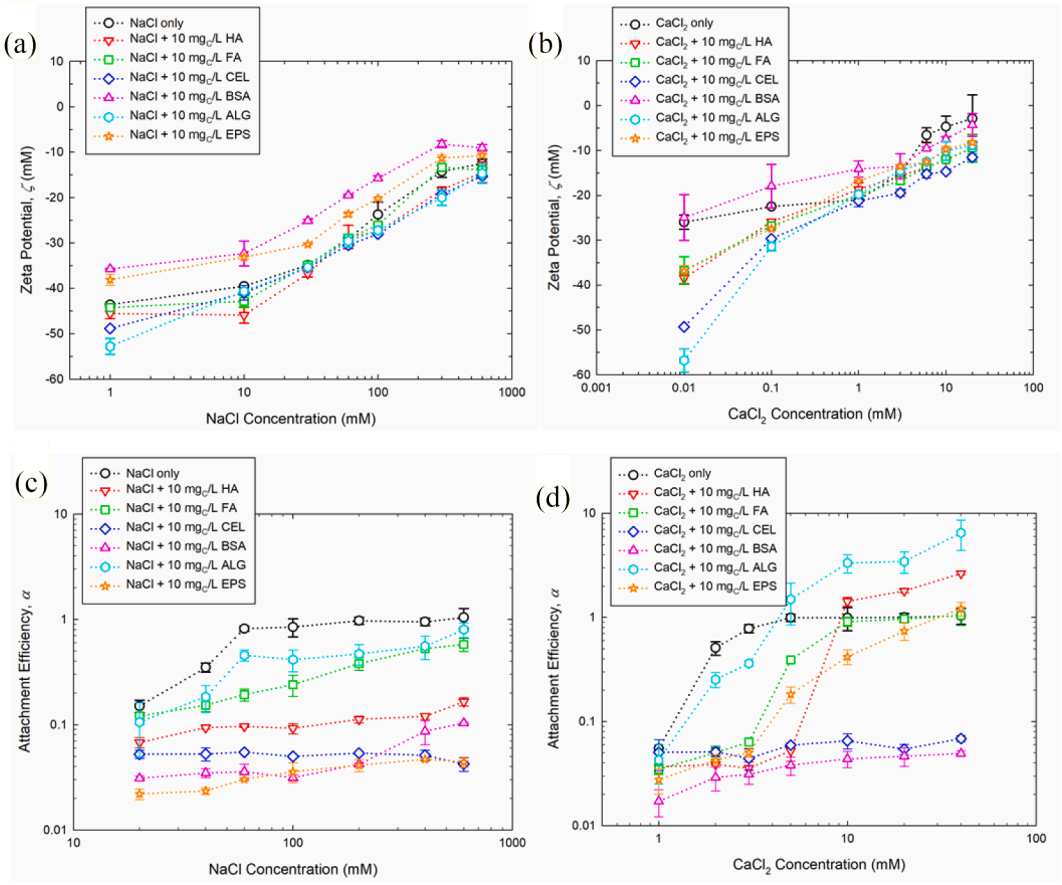

Fig. 2. Colloidal stability of NAC in electrolyte solutions at fixed macromolecule concentration: Zeta potential in the presence or absence of 10 mg_C/L macromolecules as a function of (a) NaCl and (b) $CaCl_2$ concentrations; attachment efficiency in the presence or absence of 10 mg_C/L macromolecules as a function of (c) NaCl and (d) $CaCl_2$ concentrations. The attachment efficiencies were calculated by normalizing each aggregation rate to the fast (favorable) aggregation rate obtained at high salt (NaCl or $CaCl_2$) concentrations alone. The unit of mg_C/L refers to the total organic carbon (TOC) concentration in milligram TOC per liter. All experiments were conducted at 10 mg/L NAC, pH 6, and 25 °C. The error bars represent standard deviations from triplicate samples. The dotted lines are only for visual guidance.

Our previous study determined that the EPS sample was constituted mainly of 50% proteins, followed by 25% polysaccharides and 13% uronic acids, with C, H, O, and N contents accounting for 39.6%, 5.7%, 32.5%, and 10.8%, respectively (Liu et al., 2020). Therefore, alike BSA, EPS also reduced the negative charge of NAC in NaCl solution (Fig. 2a). Compared with the spherical and compact protein structure of BSA, EPS existing as random coils with incompletely extending chains was less effective in charge reduction (Wang et al., 2012). The presence of 10 mg_C/L FA caused minimal change (<12%) on ζ potential at all NaCl concentrations. Contrarily, other macromolecules (HA, CEL, and ALG) showed overlapped trends that slightly enhanced the negative ζ potential in NaCl solution. It has been reported that the presence of HA also enhanced the negative charge of MWCNTs (Liu et al., 2016) but reduced that of C_{60} (Chae et al., 2012).

The attachment efficiencies of NAC in NaCl solution with or without 10 mg_C/L macromolecules are presented in Fig. 2c. The results show that all stability curves were lowered by macromolecules, leading to failure of NAC to display any diffusion-limited aggregation behavior ($\alpha = 1$) over the tested NaCl concentrations. The α values were reduced by up to ~100 times under such conditions. Therefore, all macromolecules stabilized NAC in NaCl solution, with such stabilization effect following the order of EPS > BSA > CEL > HA > FA > ALG.

As mentioned above, EPS and BSA showing the most obvious reduction of surface charge and strongest adsorption on NAC also stabilized it most effectively in NaCl solution, suppressing any observable aggregation with α between 0.02–0.11. The stabilization effect of CEL was slightly weaker than BSA initially, then enhanced to an extent identical with EPS as NaCl concentration increased to above 200 mM. Such aggregation behavior of NAC was unlike MWCNTs, which still exhibited diffusion-limited aggregation regime in NaCl solution with the present of CEL that raised CCC from 25 to 210 mM NaCl (Liu et al., 2016). The presence of HA effectively suppressed aggregation of NAC similar to C_{60} (Chen and Elimelech, 2007; Zhang et al., 2013) and SWCNTs (Saleh et al., 2010) in NaCl solution by lowering α to an order of magnitude. However, FA showed stronger stabilization effect on NAC than C_{60} (Zhang et al., 2013) and soot (Chen et al., 2019), as α continuously increased from 0.19 to 0.58 yet never reached unity as NaCl concentration rising from 60 to 600 mM. Although ALG enhanced the negative charge of NAC in NaCl solution (Fig. 2a), it exhibited the weakest stabilization effect among all macromolecules ($\alpha = 0.80$ at 600 mM NaCl), shifting the stability curve downwards while maintaining a shape most alike the curve measured without macromolecule (Fig. 2c).

3.2.2. *$CaCl_2$ solutions*

Fig. 2b shows that the macromolecular influence on ζ potential of NAC was more prominent at lower $CaCl_2$ concentrations, which was likely attributed to the sensitivity of particle negative charge to high Ca^{2+} concentration that diminished the macromolecular effects. Over the tested $CaCl_2$ concentrations, BSA still exhibited the most significant reduction of negative charge on NAC among all macromolecules. However, BSA only reduced the negative charge at 0.01–3 mM $CaCl_2$, while enhanced it at 6–20 mM $CaCl_2$. This concentration-dependent effect of BSA in $CaCl_2$ solution was different from that observed in NaCl solution (Fig. 2a) and in other studies, which reported monotonic

charge screening effect on particles over a wide range of $CaCl_2$ concentrations (e.g., 0.5–30 mM) (Chen et al., 2019; Liu et al., 2018). Similar to the results obtained in NaCl solution, CEL and ALG enhanced the negative charge of NAC especially at low electrolyte concentrations. Notably, the most negative ζ potential was attained at 0.01 mM $CaCl_2$ in the presence of 10 mg_C/L ALG, which enhanced it from −26.0 to −56.8 mV. The ζ potentials of NAC in the presence of other macromolecules (HA, FA, and EPS) showed overlapped trends, which were reduced at 0.4–3 mM $CaCl_2$ while enhanced at other concentrations.

The attachment efficiencies of NAC with or without 10 mg_C/L macromolecules were determined at various $CaCl_2$ concentrations (Fig. 2d). Unlike the stabilization results in NaCl solution, NAC was significantly destabilized by 10 mg_C/L ALG and HA at $CaCl_2$ concentrations above 5 and 10 mM, respectively. The α values exceeded 1 under these conditions and reached up to 6.5 and 2.6 in the presence of 10 mg_C/L ALG and HA, respectively, at 40 mM $CaCl_2$, indicating non-DLVO interactions. The stronger destabilization effect of ALG than HA was confirmed by visual observation, which shows that NAC formed apparent flocs at high $CaCl_2$ concentrations (10, 20, and 40 mM) in the presence of ALG (Fig. S5e) but not HA (Fig. S5a). However, their destabilization effect on NAC reversed to stabilization below 5 mM $CaCl_2$. For instance, the aggregation rate of NAC was reduced by up to 22 times in the presence of HA at 3 mM $CaCl_2$. The complex effects of ALG depending on $CaCl_2$ concentration have been reported for C_{60} (Saleh et al., 2010), soot (Chen et al., 2019), and graphene (Su et al., 2018). Similar results were also reported for HA on stability of C_{60} (Chen and Elimelech, 2007) and biochar (Yang et al., 2019).

Different from ALG and HA, other 4 macromolecules mainly stabilized NAC in $CaCl_2$ solution following the order of BSA > CEL > EPS > FA (Fig. 2d). The presence of 10 mg_C/L FA only stabilized NAC at $CaCl_2$ concentration below 10 mM. Similarly, EPS also stabilized NAC most effectively at $CaCl_2$ concentrations near the CCC (3.1 mM), while such effect weakened at higher $CaCl_2$ concentration and disappeared at 40 mM $CaCl_2$. This stabilization effect of EPS depending on $CaCl_2$ concentration was different from its strong stabilization effect in NaCl solution that was independent of electrolyte concentration (Fig. 2c). However, CEL and BSA still exhibited the strongest stabilization effect in $CaCl_2$ solution as similarly in NaCl solution, suppressing NAC aggregation ($\alpha <$ 0.07) at all electrolyte concentrations. It has been observed differently for MWCNTs that showed both reaction- and diffusion-limited aggregation regimes in $CaCl_2$ solution when CEL was present, raising CCC from 0.9 to 2.7 mM (Liu et al., 2016). Except for ALG, other 5 macromolecules did not induce any apparent flocculation that could be visually observed in suspensions containing NAC and $CaCl_2$ (Fig. S5).

3.3. Stability in macromolecule solution at fixed electrolyte concentration

The attachment efficiency as a function of macromolecule concentration was further determined at two fixed electrolyte concentrations near CCC and seawater levels (Fig. 3). Under all tested conditions, macromolecules stabilized NAC and such effect generally enhanced with increasing macromolecule concentration (Fig. 3a–c), except for HA and ALG present at 10 mM $CaCl_2$ that destabilized NAC (Fig. 3d).

At 60 mM NaCl (Fig. 3a), CEL and BSA displayed strong stabilization effect that was generally unaffected by macromolecule concentrations. However, HA and EPS showed weaker stabilization effect that gradually enhanced with their concentrations. At 10 mg_C/L, CEL, BSA, and EPS effectively stabilized NAC to similar extents. Negligible influence was observed for ALG at any concentration. The α values for 10 mg_C/L HA, 1–10 mg_C/L CEL and BSA, and 2.5–10 mg_C/L EPS were below 0.1, which generally correlates to negligible particle aggregation (Chen and Huang, 2017).

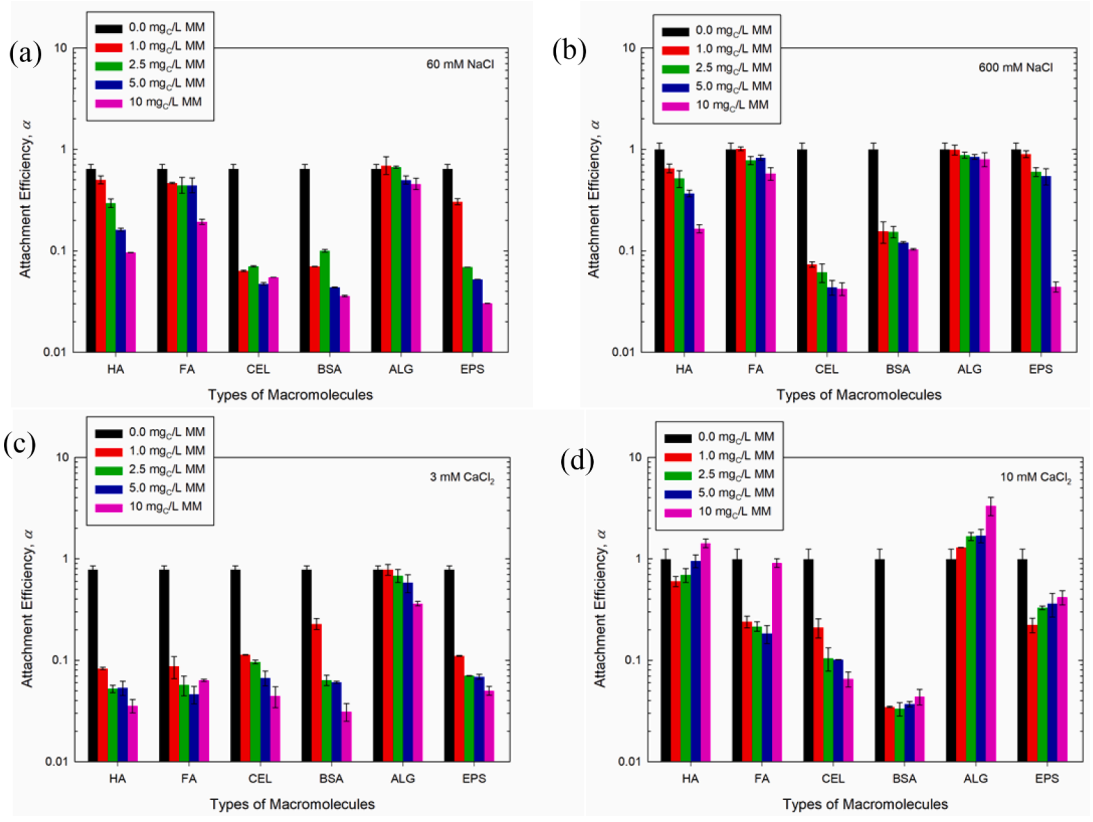

Fig. 3. Attachment efficiency of NAC as a function of macromolecule concentration determined at (a) 60 mM NaCl, (b) 600 mM NaCl, (c) 3 mM $CaCl_2$, and (d) 10 mM $CaCl_2$. The attachment efficiencies were calculated by normalizing each aggregation rate to the fast (favorable) aggregation rate obtained at high salt (NaCl or $CaCl_2$) concentrations alone (i.e., 0 mg_C/L macromolecule (MM)). The unit of mg_C/L refers to the total organic carbon (TOC) concentration in milligram TOC per liter. All experiments were conducted at 10 mg/L NAC, pH 6, and 25 °C. The error bars represent standard deviations of triplicate samples.

At 600 mM NaCl (Fig. 3b), no aggregation was observed at any concentrations of CEL or BSA, as well as 10 mg_C/L of EPS or HA. At both tested NaCl concentrations, the stabilization effects of HA and EPS significantly enhanced with increasing macromolecule concentration. For instance, α decreased by an order of magnitude as EPS concentration increased from 5 to 10 mg_C/L, indicating that fast aggregation was completely inhibited. The enhanced stabilization effect due to increased macromolecule concentration was also reported for other ENM such as MWCNTs (Yang et al., 2017), biochar (Yang et al., 2019), and GO (Ali et al., 2020). By contrast, CEL, BSA, and ALG showed effects independent of macromolecule concentration and their results represented two extreme cases: CEL and BSA stabilized NAC even under low macromolecule concentrations, whereas ALG exhibited negligible effect at high macromolecule concentrations.

Among these 4 electrolyte concentrations, the stabilization effect of macromolecules was the most obvious at 3 mM $CaCl_2$ (Fig. 3c). Except for ALG, other 5 macromolecules strongly stabilized NAC to similar extents and their stabilization effects enhanced with macromolecule concentration. These results were consistent with those presented in Fig. 2d at 3 mM $CaCl_2$, further showing that these 5 macromolecules effectively stabilized NAC even at 1 mg_C/L. In comparison, the stabilization effect of ALG only became obvious at 10 mg_C/L.

More complex results were found at 10 mM $CaCl_2$ where stabilization or destabilization effects occurred depending on the type and

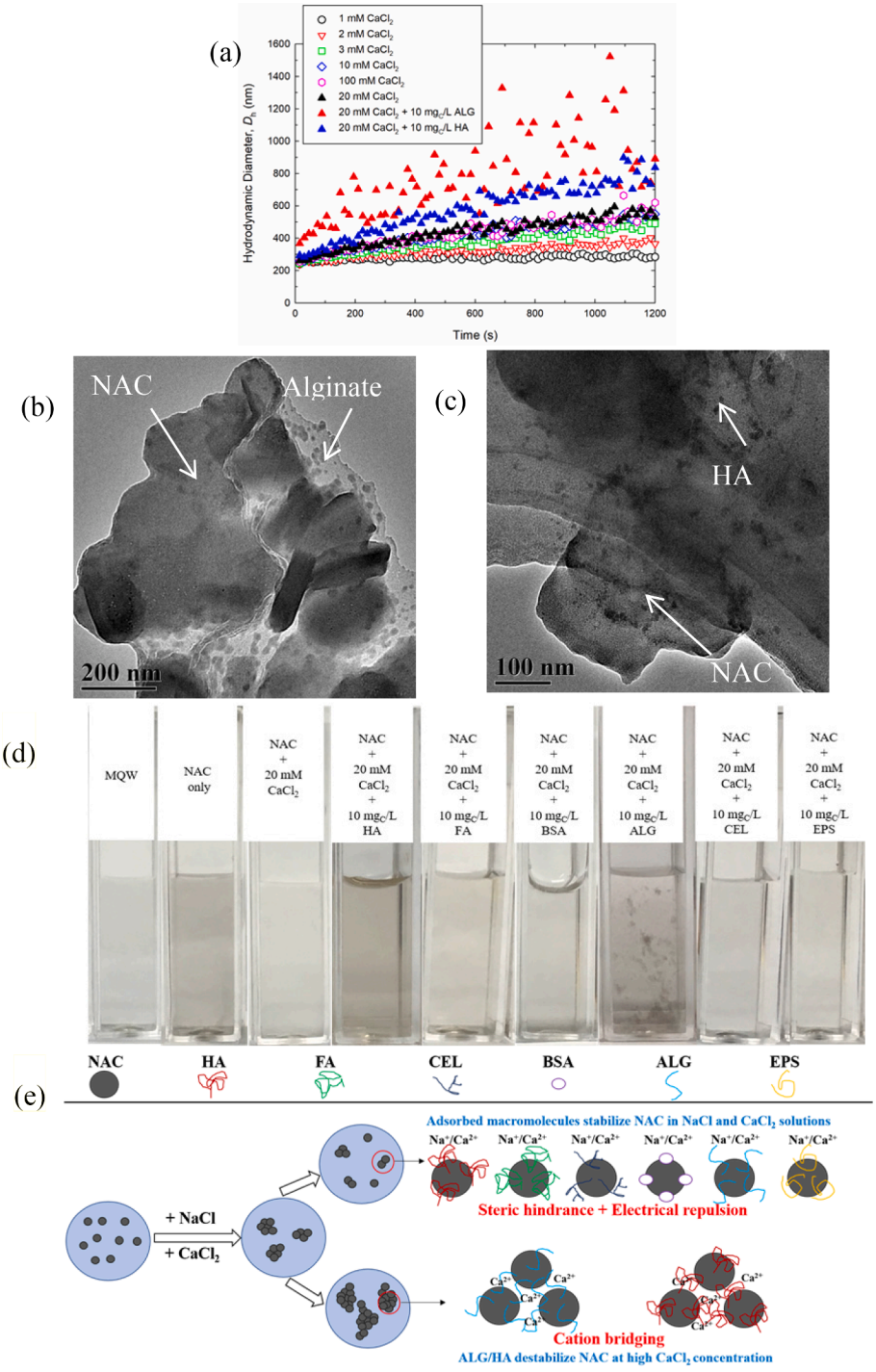

Fig. 4. (a) Representative aggregation profiles of NAC at various $CaCl_2$ concentrations in the absence or presence of 10 mg_C/L ALG or HA; transmission electron micrograph (TEM) images showing NAC after 20 min contact with (b) 10 mM $CaCl_2$ and 10 mg_C/L ALG, and (c) 10 mM $CaCl_2$ and 10 mg_C/L HA; (d) visual observations for NAC in the presence or absence of $CaCl_2$ and different macromolecules; (e) stabilizing and destabilizing mechanisms of NAC by macromolecules. The unit of mg_C/L refers to the total organic carbon (TOC) concentration in milligram TOC per liter. All experiments were conducted at 10 mg/L NAC, pH 6, and 25 °C.

concentration of macromolecules (Fig. 3d). At this $CaCl_2$ concentration, CEL and BSA still strongly stabilized NAC as observed above at other 3 electrolyte concentrations. Although EPS stabilized NAC at 1–10 mg_C/L, its effect slightly weakened with increasing macromolecule concentration. This was also observed when FA and HA increased from 5 to 10 and 1 to 5 mg_C/L, respectively. It was noted that 10 mg_C/L HA and 1–10 mg_C/L ALG destabilized NAC in 10 mM $CaCl_2$ solution (Fig. 3d). The results indicate that HA may stabilize NAC at low HA concentration (e.g., 1–5 mg_C/L) under seawater $CaCl_2$ conditions, while destabilize NAC at high HA concentration (e.g., 10 mg_C/L). Similar result was previously reported that HA stabilized biochar at 0.5–2.5 mg_C/L, but promoted its aggregation at 5 mg_C/L (Yang et al., 2019). Different from HA, ALG significantly destabilized NAC at all macromolecule concentrations under seawater $CaCl_2$ condition, with the effect enhancing with both the concentrations of ALG (Fig. 3d) and $CaCl_2$ (Fig. 2d).

3.4. Interaction mechanisms between NAC and macromolecules

3.4.1. Stabilization mechanisms

Enhanced electrical repulsion and steric hindrance were two major stabilization mechanisms responsible for inhibiting NAC aggregation by macromolecules. However, the contribution of these stabilization mechanisms was dependent upon the type and concentration of both macromolecules and electrolytes. The proposed stabilization mechanisms are illustrated in Fig. 4e.

At most NaCl and $CaCl_2$ concentrations, CEL effectively enhanced the negative charge of NAC and inhibited aggregation (Fig. 2), displaying stronger stabilization effect at higher CEL concentration (Fig. 3). Dispersed NAC from 10 mM $CaCl_2$ solution could be observed under TEM (Fig. S6i). The strong negative charge of CEL resulted in the lowest adsorption (q_e= 18.8 ± 3.6 mg_C/g (Table 1)) onto NAC among all macromolecules due to electrical repulsion (Liu et al., 2016). Therefore, enhanced electrical repulsion of NAC by CEL was mainly responsible for its stabilization.

Similarly, HA and FA also enhanced the negative ζ potential of NAC (Fig. 2a, b), contributing to their stabilization. These two humic substances were recognized to contain high concentrations of negatively charged (e.g., carboxylic and phenolic) functional groups (Zhang et al., 2013), which would deprotonate to enhance the charge of NAC. However, electrostatic interaction was not likely the sole stabilization mechanism, since the charge did not change apparently especially by FA in NaCl solution (Fig. 2a). Table 1 shows that the adsorption affinity of macromolecules followed the order of BSA > FA > ALG > EPS > HA > CEL. The semi-rigid HA and FA macromolecules adsorbed onto the hydrophobic NAC surface provided steric hindrance (Fig. 4e), preventing NAC aggregation as have been similarly reported for SWCNTs (Saleh et al., 2010), MWCNTs (Saleh et al., 2008), C_{60} (Zhang et al., 2013), and soot (Chen et al., 2019). Dispersed NAC with surface coating were observed under TEM for solutions containing FA and $CaCl_2$ (Fig. S6g, h). The stronger stabilization effect of HA than FA in most solutions was likely attributed to the higher molecular weight, longer carbon chain, and more compact structure of HA (Ali et al., 2020). Therefore, enhanced electrostatic repulsion and steric hindrance were two major stabilization mechanisms for HA and FA.

Steric hindrance highly depends on macromolecule structure and its adsorption affinity onto NAC. The adsorption experiment revealed that BSA exhibited the strongest adsorption by NAC among 6 macromolecules (Table 1). As mentioned earlier, BSA could be spontaneously adsorbed onto NAC surface (Fig. 2a, b). The hydrophobic interactions between BSA and NAC surface also promoted adsorption (Bergaoui et al., 2017). Furthermore, BSA adsorbed onto NAC surface underwent structural rearrangements to gain higher conformational entropy in the protein molecule, resulting in a more compact globular architecture of BSA (Liu et al., 2020). The globular protein layer of BSA attached on NAC induced longer-range steric hindrance force than other relatively more linear macromolecules such as HA and ALG (Chen et al., 2019; Liu et al., 2018). Therefore, BSA stabilized NAC most effectively among all macromolecules via steric hindrance.

The extracted EPS sample consisted of ~50% protein and ~25% polysaccharide, and usually exists as random coils with partly extending chains under neural conditions (Wang et al., 2012). Therefore, EPS also induced charge-reduction (Fig. 2a) and strong stabilization (Figs. 2a and 3a) of NAC to a similar extent with BSA in NaCl solution via steric hindrance. However, the stabilization effect of EPS gradually disappeared as $CaCl_2$ concentration increased (Fig. 2d), which may be related to the polysaccharide content that concurrently destabilized NAC as discussed later.

Although ALG provided the strongest charge enhancement (Fig. 2a, b) of NAC and exhibited strong adsorption (Table 1), its stabilization effect was mostly negligible (Figs. 2c, d and 3a–c). This was likely attributed to its destabilization effect as discussed below that counterbalanced or overcame stabilization.

3.4.2. Destabilization mechanism

Fig. 4a presents the aggregation profiles of NAC in $CaCl_2$ solutions with or without 10 mg_C/L ALG or HA. The aggregation rate of NAC increased with $CaCl_2$ concentration from 1 to 3 mM, while remained unchanged when further increased to 100 mM. This aligns with the DLVO-behavior since CCC was determined as 3.1 mM $CaCl_2$ (Fig. 1c), above which α stays at 1 (Eq. S3) under diffusion-limited condition where attraction dominates over repulsion. However, the aggregation rate was prominently elevated by 10 mg_C/L ALG or HA at 20 mM $CaCl_2$ (Fig. 4a), yielding slopes of aggregation profiles clearly above those obtained in fast aggregation regime (α> 1). This contradicts with the enhanced negative ζ potential of NAC under such conditions (Fig. 2b), indicating that electrical double layer compression was not likely the destabilization mechanism. Instead, non-DLVO interactions were responsible for destabilizing NAC, with ALG showing a stronger effect than HA by raising D_h up to ~1800 in 20 min.

The major destabilization mechanism was identified as cation bridging of ALG or HA with Ca^{2+} at high concentrations as depicted in Fig. 4e. The TEM images (Fig. 4b and S6l-n) show that ALG bridging with Ca^{2+} resulted in formation of alginate gel that enmeshed NAC and significantly promoted aggregation. It is recognized that Ca^{2+} can complex with the carboxylic groups in the guluronic acid blocks of ALG in a planar two-dimensional manner (Cerciello et al., 2017), generating cross-linked gels that destabilized graphene (Su et al., 2018) and soot (Chen et al., 2019). At $CaCl_2$ concentrations above 3 mM (near CCC), the destabilization effect enhanced with concentrations of both $CaCl_2$ (Fig. 2d) and ALG (Fig. 3d). This was likely due to the presence of more available Ca^{2+} in solution and binding sites on ALG to form large settling flocs in suspensions that could be visually observed (Fig. S5e).

The cation bridging of HA in $CaCl_2$ solution that destabilized NAC occurred by simultaneous coordination of Ca^{2+} with two carboxylic groups on HA to form HA-Ca^{2+} complex (Li et al., 2020; Yang et al., 2019). The interaction between HA-Ca^{2+} complexes via hydrogen bonds generated larger molecular layer, which formed ionic bridges with the negatively charged surface sites of NAC and resulted in destabilization (Fig. 4c and S6c–f) (Zhao et al., 2019). The role of HA on NAC in $CaCl_2$ solution was governed by the interplay between destabilization and stabilization effects (Fig. 4e). Below 10 mM $CaCl_2$, HA stabilized NAC at all tested macromolecule concentrations by enhanced electrical repulsion and steric hindrance (Figs. 2b, d, and 3c). At 10 mM $CaCl_2$ and HA concentrations below 10 mg_C/L, most HA were adsorbed on NAC so that the stabilization effect dominated over or counterbalanced destabilization (Fig. 3d). At 10 mM $CaCl_2$ and 10 mg_C/L HA, free HA present in solution could bind with Ca^{2+} to form network clusters (Yu et al., 2019), leading to an overall destabilization effect.

It was noted that the stabilization effect of EPS gradually diminished at higher $CaCl_2$ concentrations, and even reversed to slight destabilization at 40 mM $CaCl_2$ (Fig. 2d). This indicates that the ~25% polysaccharide content on EPS may be similar with ALG that destabilized

NAC via cation bridging with Ca^{2+} present at high concentration, which competed with the stabilization effect of EPS (Liu et al., 2020).

3.5. Colloidal stability in NW samples

3.5.1. Early-stage stability

The colloidal stability of NAC was further studied in 6 NW samples that represent freshwater possessing different chemical properties. The pH was near 2.6 for NW1 and NW2 while above 5.21 for other samples; meanwhile, the highest cation concentrations were detected in NW1 and NW2, whereas NW3 contained the highest Ca^{2+} concentration due to liming process (Tables 2 and S6). The reasons for variation in pH and IS among 6 NW samples are explained in Fig. S2 and S1.2.3 of the Supplementary Material.

The early-stage stability of NAC in NW samples followed the order of NW6 ≈ NW5 > NW4 ≈ NW3 >> NW2 ≈ NW1 (Fig. 5a–c). The sizes of NAC in NW1 (364.5 nm) and NW2 (351.4 nm) were larger than those in other samples (~300 nm) (Fig. 5a). All NW samples reduced the negative ζ potential of NAC (absolute values < 20 mV) compared to that (~-40 mV) measured in model water at 1 mM NaCl and pH 6 (Fig. S3b). Specifically, the ζ potentials of NAC in NW1 (-1.632 mV) and NW2 (-1.625 mV) were much less negative than in other samples (Fig. 5b). These results were reasonable since both the lowest pH (~2.6) and highest cation concentrations in NW1 and NW2 (Table 2) would screen the negative charge of NAC, promoting aggregation that resulted in increased D_h and PDI. The high conductivity of NW1-3 likely correlated to their low pH and high IS (Table 2). Positive correlation was found between |ζ potential| (absolute value of ζ potential) and pH, whereas negative correlations existed between |ζ potential| and IS or conductivity (Fig. S7a–d).

The early-stage aggregation profiles in NW samples show that NAC underwent fast aggregation in NW1 and NW2 to ~1000 nm in 20 min,

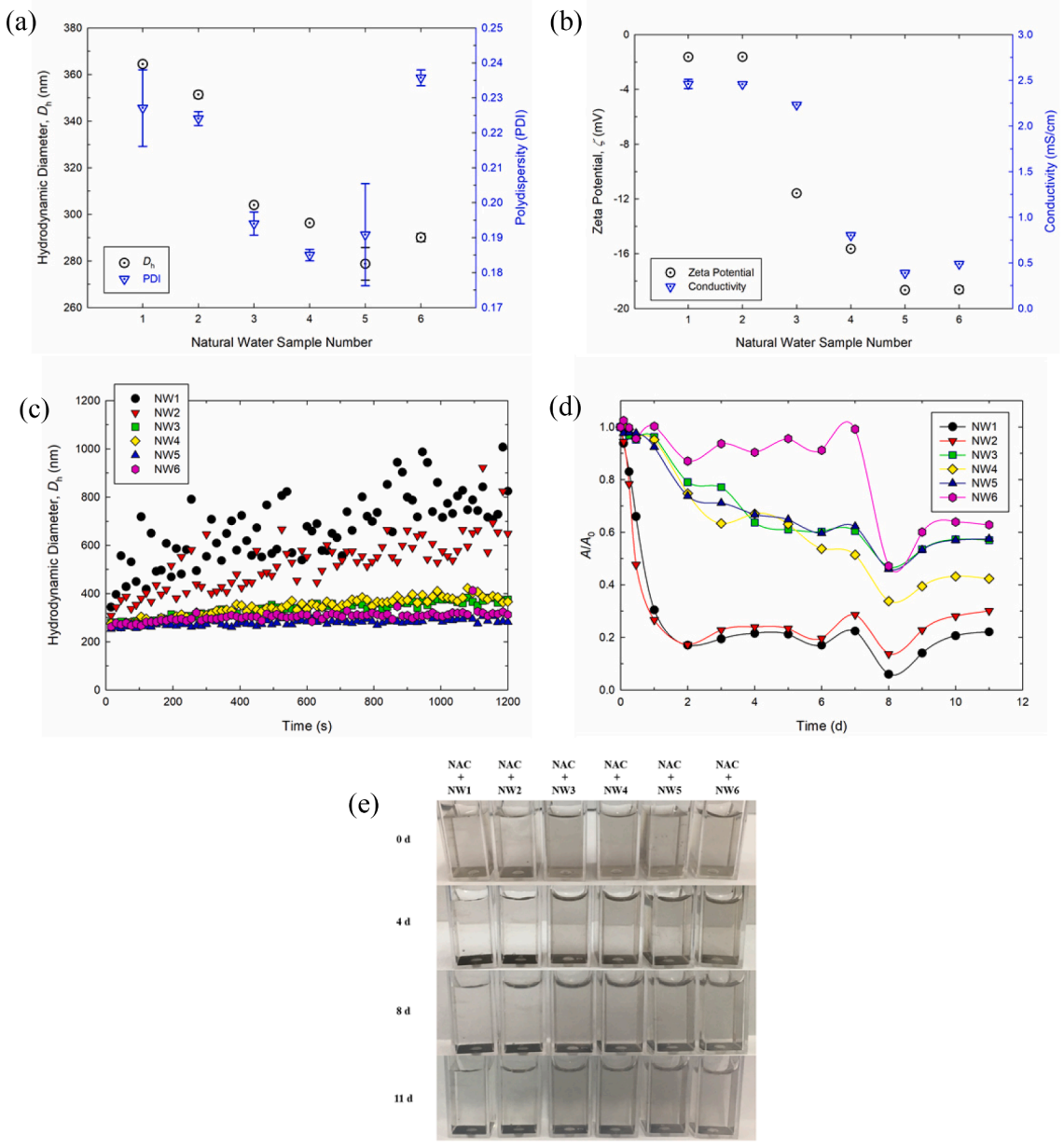

Fig. 5. Colloidal stability of NAC in different natural water (NW) samples: (a) Hydrodynamic diameter and polydispersity as well as (b) zeta potential and conductivity measured immediately after mixing NAC suspension with NW samples; (c) aggregation profiles of NAC in 6 NW samples in 20 min; (d) change in relative light absorbance (A/A_0) and visual observation of suspensions containing NAC and NW samples over 11 d All experiments were conducted at 10 mg/L NAC and 25 °C.

slightly aggregated in NW3 and NW4, while remained stable in NW5 and NW6 (Fig. 5c). Table 2 shows that NW1 and NW2 contained Ca^{2+} and Mg^{2+} concentrations about 1.5 times as their CCC (3.1 mM $CaCl_2$ and 3.3 mM $MgCl_2$) at pH 6 (Fig. 1c); meanwhile, the strongly acidic condition and the presence of ~2 mM Al^{3+} also promoted NAC aggregation. Although high Ca^{2+} concentrations were detected in NW3 (13.04 mM) and NW4 (3.790 mM), NAC remained relatively stable in these two samples possibly due to their high TOC concentrations of 41.92 and 16.28 mg/L, respectively (Table 2). These TOC concentrations were much higher than the 10 mg_C/L macromolecule concentration used in model water (Figs. 2 and 3), which may correlate to macromolecules that stabilized NAC via steric hindrance as aforementioned (Fig. 4e). Since NW5 and NW6 contained low ionic concentrations, neutral pH, and low TOC (Table 2), NAC reasonably showed strong stability in these samples. Correlation analyses further show that aggregation rate (k) increased with decreasing pH and increasing electrolyte concentrations, and were complexly influenced by macromolecules as reflected by TOC (Fig. S7e–h).

3.5.2. *Long-term stability*

The long-term stability of NAC in NW samples was investigated by measuring the light absorbance (Fig. 5d) and visual observation (Fig. 5e) of suspensions over 11 d Generally similar long-term stability results were observed for NAC as compared with the early-stage experiments, following the order of NW6 > NW5 ≈ NW3 > NW4 >> NW2 ≈ NW1.

The change in relative light absorbance (A/A_0) in Fig. 5d reflects the proportion of NAC remaining suspended in NW samples. It shows that NW1 and NW2 significantly destabilized NAC by inducing ~83% reduction in A/A_0 in 2 d, which was consistent with their clear suspensions visually observed in Fig. 5e, indicating fast sedimentation of NAC. However, NAC settled gradually in other NW samples as reflected from both their slowly decreasing A/A_0 and dark suspensions. After 7 d, A/A_0 decreased to 0.5–0.6 in NW3–5, yet remained above 0.9 in NW6. The A/A_0 values became stable in 11 d, upon which near 20%, 30%, and 40% of NAC remained suspending in NW1, NW2, and NW4, respectively, while 50–60% of NAC remained suspending in other samples.

Compared with NAC, a previous study reported stronger stability of GO nanomaterial in NW samples, with above 90% particles remained suspending in Calls Creek water after 28 d (Chowdhury et al., 2013). The solution chemistry of Calls Creek water (pH = 7.9, conductivity = 26 μS/cm, and TOC = 2.8 mg/L) was similar to NW5 (pH = 7.67, conductivity = 387 μS/cm, and TOC = 1.2 mg/L). As conductivity mainly correlates to electrolyte concentration, the lower conductivity of Calls Creek water than NW5 sample may be responsible for causing a greater ζ potential of GO (−35.4 mV) than NAC (−18.6 mV), thereby resulting in the stronger stability of GO.

4. Conclusion

The results indicate that the colloidal stability of NAC was governed by the complex interplay among solution pH, electrolytes, and macromolecules. In model aqueous solutions, higher pH stabilized NAC by raising CCC from 28 to 590 mM NaCl due to enhanced electrical repulsion. Increased cation concentration destabilized NAC by charge screening with the effect following $Ba^{2+} > Ca^{2+} > Mg^{2+} >> Na^{+} > K^{+}$. The aggregation behavior could be predicted by DLVO model with a Hamaker constant (A_{CWC}) of 4.3×10^{-20} J. Macromolecules stabilized NAC in 20–600 mM NaCl solutions at 10 mg_C/L, with the order of EPS > BSA > CEL > HA > FA > ALG. Enhanced electrical repulsion and steric hindrance, which originated from adsorbed macromolecule layer and was affected by macromolecule structure, were two major stabilization mechanisms. Most macromolecules still stabilized NAC in $CaCl_2$ solution, except for ALG and HA that significantly destabilized NAC due to cation bridging with Ca^{2+} at high concentrations. Long-term stability experiments in NW samples showed that half of NAC particles remained stably suspended for ~10 d in neutral freshwater. However, NAC may undergo rapid aggregation and sedimentation in acidic or saline aquatic environments depending on the type and concentration of macromolecules present.

Declaration of Competing Interest

The authors declare that they have no known competing financial interests or personal relationships that could have appeared to influence the work reported in this paper.

Acknowledgments

This work was supported by Guangdong Basic and Applied Basic Research Foundation [Grant No. 2021A1515011503]; Program for Guangdong Introducing Innovative and Enterpreneurial Teams [Grant No. 2019ZT08N291]; National Natural Science Foundation of China (NSFC) [Grant No. 41807451]; Science and Technology Planning Project of Guangzhou [Grant No 202002020072]; and Guangzhou Young Talents Lifting Program [Grant No. X20200301025].

Supplementary materials

Supplementary materials associated with this article can be found online, which include: S1. Additional Details on Materials and Methods; S2. Additional 8 Figures; and S3. Additional 6 Tables, in the online version, at doi:10.1016/j.watres.2021.117561.

References

Abdulkareem-Alsultan, G., Asikin-Mijan, N., Lee, H.V., Taufiq-Yap, Y.H., 2016. A new route for the synthesis of La-Ca oxide supported on nano activated carbon via vacuum impregnation method for one pot esterification-transesterification reaction. Chem. Eng. J. 304, 61–71.

Ali, J., Li, Y., Wang, X., Zhao, J., Xi, N., Zhang, Z., Xia, X., 2020. Climate-zone-dependent effect mechanism of humic acid and fulvic acid extracted from river sediments on aggregation behavior of graphene oxide. Sci. Total Environ. 721, 137682.

Bergaoui, M., Aguir, C., Khalfaoui, M., Enciso, E., Duclaux, L., Reinert, L., Fierro, J.L.G., 2017. New insights in the adsorption of bovine serum albumin onto carbon nanoparticles derived from organic resin: experimental and theoretical studies. Microporous Mesoporous Mater. 241, 418–428.

Bonvin, F., Jost, L., Randin, L., Bonvin, E., Kohn, T., 2016. Super-fine powdered activated carbon (SPAC) for efficient removal of micropollutants from wastewater treatment plant effluent. Water Res. 90, 90–99.

Cerciello, A., Del Gaudio, P., Granata, V., Sala, M., Aquino, R.P., Russo, P., 2017. Synergistic effect of divalent cations in improving technological properties of cross-linked alginate beads. Int. J. Biol. Macromol. 101, 100–106.

Chae, S.R., Xiao, Y., Lin, S., Noeiaghaei, T., Kim, J.O., Wiesner, M.R., 2012. Effects of humic acid and electrolytes on photocatalytic reactivity and transport of carbon nanoparticle aggregates in water. Water Res. 46 (13), 4053–4062.

Chen, C., Geng, X., Huang, W., 2017. Adsorption of 4-chlorophenol and aniline by nanosized activated carbons. Chem. Eng. J. 327, 941–952.

Chen, C., Huang, W., 2017. Aggregation kinetics of nanosized activated carbons in aquatic environments. Chem. Eng. J. 313, 882–889.

Chen, C., Wei, J., Li, J., Duan, Z., Huang, W., 2019. Influence of macromolecules on aggregation kinetics of diesel soot nanoparticles in aquatic environments. Environ. Pollut. 252 (Pt B), 1892–1901.

Chen, K.L., Elimelech, M., 2007. Influence of humic acid on the aggregation kinetics of fullerene (C_{60}) nanoparticles in monovalent and divalent electrolyte solutions. J. Colloid Interface Sci. 309 (1), 126–134.

Chowdhury, I., Duch, M.C., Mansukhani, N.D., Hersam, M.C., Bouchard, D., 2013. Colloidal properties and stability of graphene oxide nanomaterials in the aquatic environment. Environ. Sci. Technol. 47 (12), 6288–6296.

Hewitt, R.E., Chappell, H.F., Powell, J.J., 2020. Small and dangerous? Potential toxicity mechanisms of common exposure particles and nanoparticles. Curr. Opinion Toxicol. 19, 93–98.

Hosseini, S.M., Amini, S.H., Khodabakhshi, A.R., Bagheripour, E., Van der Bruggen, B., 2018. Activated carbon nanoparticles entrapped mixed matrix polyethersulfone based nanofiltration membrane for sulfate and copper removal from water. J. Taiwan Inst. Chem. Eng. 82, 169–178.

Kopac, T., Bozgeyik, K., Flahaut, E., 2018. Adsorption and interactions of the bovine serum albumin-double walled carbon nanotube system. J. Mol. Liq. 252, 1–8.

Kyzyma, O.A., Avdeev, M.V., Bolshakova, O.I., Melentev, P., Sarantseva, S.V., Ivankov, O.I., Korobov, M.V., Mikheev, I.V., Tropin, T.V., Kubovcikova, M., Kopcansky, P., Korolovych, V.F., Aksenov, V.L., Bulavin, L.A., 2019. State of aggregation and toxicity of aqueous fullerene solutions. Appl. Surf. Sci. 483, 69–75.

Lakshmi, S.D., Avti, P.K., Hegde, G., 2018. Activated carbon nanoparticles from biowaste as new generation antimicrobial agents: a review. Nano Struct. Nano Objects 16, 306–321.
László, K., Tombácz, E., Kerepesi, P., 2004. Surface chemistry of nanoporous carbon and the effect of pH on adsorption from aqueous phenol and 2,3,4-trichlorophenol solutions. Colloids Surf. A Physicochem. Eng. Asp. 230 (1–3), 13–22.
László, K., Tombácz, E., Novák, C., 2007. pH-dependent adsorption and desorption of phenol and aniline on basic activated carbon. Colloids Surf. A Physicochem. Eng. Asp. 306 (1–3), 95–101.
Li, B., He, X., Wang, P., Liu, Q., Qiu, W., Ma, J., 2020. Opposite impacts of K^+ and Ca^{2+} on membrane fouling by humic acid and cleaning process: evaluation and mechanism investigation. Water Res. 183, 116006.
Li, J., Yang, X., Zhang, Z., Xiao, H., Sun, W., Huang, W., Li, Y., Chen, C., Sun, Y., 2021. Aggregation kinetics of diesel soot nanoparticles in artificial and human sweat solutions: effects of sweat constituents, pH, and temperature. J. Hazard. Mater. 403, 123614.
Liu, W., Zhao, X., Cai, Z., Han, B., Zhao, D., 2016. Aggregation and stabilization of multiwalled carbon nanotubes in aqueous suspensions: influences of carboxymethyl cellulose, starch and humic acid. RSC Adv. 6 (71), 67260–67270.
Liu, Y., Huang, Z., Zhou, J., Tang, J., Yang, C., Chen, C., Huang, W., Dang, Z., 2020. Influence of environmental and biological macromolecules on aggregation kinetics of nanoplastics in aquatic systems. Water Res. 186, 116316.
Liu, Y., Yang, T., Wang, L., Huang, Z., Li, J., Cheng, H., Jiang, J., Pang, S., Qi, J., Ma, J., 2018. Interpreting the effects of natural organic matter on antimicrobial activity of Ag_2S nanoparticles with soft particle theory. Water Res. 145, 12–20.
Nazem, M.A., Zare, M.H., Shirazia, S., 2020. Preparation and optimization of activated nanocarbon production using physical activation by water steam from agricultural wastes. RSC Adv. 10, 1463–1475.
Partlan, E., Davis, K., Ren, Y., Apul, O.G., Mefford, O.T., Karanfil, T., Ladner, D.A., 2016. Effect of bead milling on chemical and physical characteristics of activated carbons pulverized to superfine sizes. Water Res. 89, 161–170.
Saleh, N.B., Pfefferle, L.D., Elimelech, M., 2008. Aggregation kinetics of multiwalled carbon nanotubes in aquatic systems: measurements and environmental implications. Environ. Sci. Technol. (42), 7963–7969.
Saleh, N.B., Pfefferle, L.D., Elimelech, M., 2010. Influence of biomacromolecules and humic acid on the aggregation kinetics of single-walled carbon nanotubues. Environ. Sci. Technol. 44, 2412–2418.
Sengupta, A., Kelly, S.C., Dwivedi, N., Thadhani, N., Prausnitz, M.R., 2014. Efficient intracellular delivery of molecules with high cell viability using nanosecond-pulsed laser-activated carbon nanoparticles. ACS Nano 8 (3), 2889–2899.
Su, Y., Huang, C., Lu, F., Tong, X., Niu, J., Mao, L., 2018. Alginate affects agglomeration state and uptake of ^{14}C-labeled few-layer graphene by freshwater snails: implications for the environmental fate of graphene in aquatic systems. Environ. Pollut. 234, 513–522.
Tang, H., Zhao, Y., Yang, X., Liu, D., Shao, P., Zhu, Z., Shan, S., Cui, F., Xing, B., 2017. New insight into the aggregation of graphene oxide using molecular dynamics simulations and extended derjaguin-landau-verwey-overbeek theory. Environ. Sci. Technol. 51 (17), 9674–9682.
Updegraff, D.M., 1969. Semimicro determination of cellulose inbiological material. Anal. Biochem. 32 (3), 420–424.
Vidal, L., Chisvert, A., Canals, A., Psillakis, E., Lapkin, A., Acosta, F., Edler, K.J., Holdaway, J.A., Marken, F., 2008. Chemically surface-modified carbon nanoparticle carrier for phenolic pollutants: extraction and electrochemical determination of benzophenone-3 and triclosan. Anal. Chim. Acta 616 (1), 28–35.
Wang, H., Zhao, X., Han, X., Tang, Z., Liu, S., Guo, W., Deng, C., Guo, Q., Wang, H., Wu, F., Meng, X., Giesy, J.P., 2017. Effects of monovalent and divalent metal cations on the aggregation and suspension of Fe_3O_4 magnetic nanoparticles in aqueous solution. Sci. Total Environ. 586, 817–826.
Wang, L.L., Wang, L.F., Ren, X.M., Ye, X.D., Li, W.W., Yuan, S.J., Sun, M., Sheng, G.P., Yu, H.Q., Wang, X.K., 2012. pH dependence of structure and surface properties of microbial EPS. Environ. Sci. Technol. 46 (2), 737–744.
Xia, T., Guo, X., Lin, Y., Xin, B., Li, S., Yan, N., Zhu, L., 2019. Aggregation of oxidized multi-walled carbon nanotubes: interplay of nanomaterial surface O-functional groups and solution chemistry factors. Environ. Pollut. 251, 921–929.
Xu, F., Wei, C., Zeng, Q., Li, X., Alvarez, P.J.J., Li, Q., Qu, X., Zhu, D., 2017. Aggregation behavior of dissolved black carbon: implications for vertical mass flux and fractionation in aquatic systems. Environ. Sci. Technol. 51 (23), 13723–13732.
Yang, W., Shang, J., Sharma, P., Li, B., Liu, K., Flury, M., 2019. Colloidal stability and aggregation kinetics of biochar colloids: effects of pyrolysis temperature, cation type, and humic acid concentrations. Sci. Total Environ. 658, 1306–1315.
Yang, X., Wang, Q., Qu, X., Jiang, W., 2017. Bound and unbound humic acids perform different roles in the aggregation and deposition of multi-walled carbon nanotubes. Sci. Total Environ. 586, 738–745.
Yu, S., Shen, M., Li, S., Fu, Y., Zhang, D., Liu, H., Liu, J., 2019. Aggregation kinetics of different surface-modified polystyrene nanoparticles in monovalent and divalent electrolytes. Environ. Pollut. 255 (Pt 2), 113302.
Zhang, W., Rattanaudompol, U.S., Li, H., Bouchard, D., 2013. Effects of humic and fulvic acids on aggregation of aqu/nC_{60} nanoparticles. Water Res. 47 (5), 1793–1802.
Zhao, X., Wu, Y., Zhang, X., Tong, X., Yu, T., Wang, Y., Ikuno, N., Ishii, K., Hu, H., 2019. Ozonation as an efficient pretreatment method to alleviate reverse osmosis membrane fouling caused by complexes of humic acid and calcium ion. Front. Environ. Sci. Eng. 13 (4), 55.